SSM-PixNav: State Space Models for Pixel-Guided Embodied Navigation

Anonymous authors
Paper under double-blind review

Abstract

While navigating a robot towards a specific object or image, how do we ensure it focuses on the correct location we are referring to? Object goal navigation, image goal navigation, goal instance navigation and pixel navigation are popular approaches to solve the problem. In this work, we focus on pixel navigation as it solves the problem more precisely by providing the agent with additional pixel-level guidance. Prior work has largely relied on RGB input; as a result, the policy lacks explicit geometric awareness, which can be important when visually similar regions differ in navigability. Additionally, recent work leverages transformer-based architectures to model temporal dependencies in observations, thereby increasing computational cost. Another practical limitation is the absence of an open benchmark dataset to reproduce the baselines. Through this work, we address these limitations along three directions. First, we introduce an RGBD-PixNav policy, a transformer-based architecture that incorporates depth directly into the policy. Second, to improve temporal modelling while maintaining computational efficiency, we employ Mamba, a recent State Space Model (SSM) architecture that enables lightweight sequential scanning of the observations. Building on this, we develop Causal SSM-based navigation policies and introduce a depth gating mechanism to regulate the contribution of depth features during policy learning. Third, to facilitate reproducible evaluation and future research, we curate the PixNav Trajectories dataset using HM3D scenes in Habitat-sim. Through extensive experiments, we establish an RGB-only baseline and extend to a transformer-based RGBD model and SSM-based variants. Results show that the proposed Causal SSM-RGB PixNav and Causal SSM-RGBD PixNav with depth gate consistently outperform other policy variants, improving the success rate by ≈0.4 while reducing model size to just half, ≈27M parameters. The models also demonstrate robustness to observation noise and varying history length. Code and dataset will be publicly released.

1 Introduction

Robotics is an interdisciplinary field of engineering that focuses on building agents to make human life safer and more efficient. Robots can be stationary or mobile. Based on the structure, mobile robots can be wheeled, legged or flying. Navigation is an essential feature of mobile robots, enabling them to move from one point to another. Navigation is a well-studied problem in classical theory, but these solutions may not be generalizable or intelligent. In the classical approach, navigation is handled through hand-engineered components, including the path planner, Simultaneous Localization and Mapping (SLAM), and the control loop to track the agent. In essence, multiple modules are needed to complete a solution pipeline. With the emergence of AI, researchers aim to predict the best action directly based on observations to achieve a goal. These models are either vision-only or vision-language-based Zhao et al., Zhang et al. (2024), Zhang et al. (2025). These works have also facilitated the emergence of mapless navigation even with only RGB data, leveraging stronger Vision-Language Model (VLM)-based guidance. Multimodal mapping for navigation without a classical loop-closure-based approach is also being explored in Huang et al. (2023b), Huang et al. (2023a).

Embodied navigation adopts an end-to-end learning paradigm that enables agents to directly map raw observations to actions, thereby making them more adaptable to novel, unstructured, and dynamic environments. Such a paradigm shift fosters robust and semantically grounded navigation, particularly when prior maps or carefully engineered features are unavailable or unreliable. Recently, Niklasson et al. (2024) explores the possibility of leveraging the power of embodied assistive agents to help the elderly community navigate with body awareness. Similarly, works Cai et al. (2024), Zhao et al. leverage the power of foundation models Liu et al. (2024), Kirillov et al. (2023) and VLM's Li et al. (2022), OpenAI (2023), Beyer et al. (2024), Zhu et al. (2023) for efficient embodied navigation. These embodied navigation policies can be later deployed to a robot configuration similar to the agent.

Robot navigation itself can be classified into different types based on the type of goal. The goal could be a point coordinate for point-goal navigation, an object goal category in object-goal navigation Debnath et al. (2025), Chaplot et al. (2020), an image of a goal in frame for image-goal navigation, an audio clip in an audio goal navigation, and many more. This work considers pixel-goal navigation as the main task and object-goal navigation as a downstream task.

Simulators are also very crucial for training and evaluating a navigation policy. Simulators enable testing the policy without adversely affecting the agent or the environment. For a realistic environment, simulators began to rely on photorealistic datasets, such as HM3D Ramakrishnan et al. (2021) and MP3D Chang et al. (2017). These datasets cover 3D indoor scenes from an apartment. Habitat-sim Savva et al. (2019), Szot et al. (2021), Puig et al. provide highly realistic scene rendering at several thousand frames per second for indoor scenes in the datasets listed above.

When an agent is instructed to perform object goal navigation, it will move to any instance of the object (closest to the agent) in the environment. So we cannot ensure the agent will navigate to a specific instance itself. To address this, image-goal navigation uses a goal image. Here, the agent tries to reach a similar image scene, but it is unaware of the most important element needed to ensure a match. Through pixel-goal navigation, an agent is given a goal image and a 2D mask to determine which pixels to focus on. This ensures the agent can reach a location more precisely compared to other methods. Because the goal is not defined by a goal category type or coordinates, agents can navigate toward arbitrary visual targets, including dynamic or previously unseen objects. Pixel navigation policies typically learn to map sequences of observations and goal masks directly to low-level actions, effectively bypassing explicit mapping or pose tracking modules. Existing works on pixel navigation rely on datasets that are not publicly available. Also, valuable depth information that is already available is not being leveraged. Further existing architectures are transformer-based, making them less suitable for deployment on edge devices. The key contributions to pixel navigation in this work are listed below,

1. RGBD-PixNav: An RGBD-based pixel navigation policy with transformers, a direct extension of RGB-PixNav that leverages RGB images and depth information to improve scene understanding and action prediction.
2. Causal RGB-SSM PixNav: A light-weight causal RGB-based pixel navigation policy with Mamba, that relies on RGB images only to improve scene understanding and action prediction.
3. Causal RGBD-SSM PixNav: An extension of the Causal RGB-SSM PixNav model that relies on RGB images and depth maps.
4. PixNav Trajectories, an open-source dataset of trajectories curated from the HM3D environment using Habitat's oracle agent Shortest Path Follower (SPF), addressing the lack of public supervised data for pixel navigation.
5. Robustness analysis is performed by perturbing the observations with a mild Gaussian noise.
6. Comprehensive empirical analysis shows that SSM-based policies outperform transformer-based baselines across both navigation success and computational efficiency.

Through these contributions, we demonstrate that the SSM-PixNav model is an effective natural fit for embodied navigation, thereby enabling the development of efficient, generalizable and reproducible agents.

Table 1: Model performance on entire validation fold of proposed PixNav Trajectories dataset. * is marked for weights from PixNav Cai et al. (2024).

Model	Total loss	Action loss	Distance loss	Tracking loss	Action Accuracy
PixNav*	4.54	4.51	0.31	0.0005	16.81
PixNav (our baseline)	0.94	0.93	0.02	0.0005	65.41

2 Related Works

Image-goal navigation Majumdar et al. (2022) leverages the CLIP model Radford et al. (2021) and ResNet features to encode the goal and the current observation. In Majumdar et al. (2022), policy is trained through reinforcement learning, where the agent tries to learn through exploration and exploitation of its own understanding of the environment.

In prior work Cai et al. (2024), a pixel navigation policy was proposed through imitation learning. The agent relied on RGB observations and goal descriptors. Goal descriptors include a goal image and a binary mask to show the region of interest. In this model, depth information was utilized solely to identify the goal location via pinhole camera projection. Krishnan R & etal (2026) attempted to establish a depth-only model for pixel navigation. Through decision-level fusion of the logits from depth and RGB pixel navigation models, Krishnan R & etal (2026) have shown that the ensemble model outperformed the RGB variant. While recent work has shown promising results in pixel-based navigation using transformer-style policies, reproducibility and fair benchmarking remain open challenges.

To address these issues, we curate trajectories from the HM3D dataset Ramakrishnan et al. (2021) and release a balanced version of the same, referred to as the PixNav Trajectories dataset. This dataset includes diverse trajectories generated by a Shortest Path Follower (SPF) oracle agent with a turn radius of 0.5, promoting reproducibility and fair comparison of pixel navigation algorithms. Even though we tried to follow the steps shared in PixNav Cai et al. (2024) closely, the evaluation results of model weights from Cai et al. (2024) on the PixNav Trajectories dataset were subpar. Given this, we have established a baseline for the same model by fine-tuning only the three MLP heads to predict action, steps to goal and goal coordinate. The evaluation performance of both models is compared in Table 1. The validation losses and accuracy metrics indicate that our PixNav Trajectories dataset differs from the one used by the authors of Cai et al. (2024).

3 Proposed Models for Pixel-Guided Navigation

3.1 Problem statement

In pixel navigation, the agent is exposed to several trajectories to learn how to step/move in a supervised setting. The trajectories are limited to a maximum step count of 64 due to computational complexity. The agent is allowed to take 6 valid actions: {`stop`, `forward`, `left`, `right`, `look up`, `look down`}. Given a goal image and binary mask for pixel coordinates and observations from each step, a policy is trained for an embodied agent to predict the next best action. Learning is conducted in a supervised setting using the proposed PixNav Trajectories dataset. We can further formulate this as a multi-head classification and regression problem.

3.2 Transformer-based Models for Pixel-guided Navigation

Transformers Vaswani et al. (2017), unlike RNNs and LSTMs, can model long-range dependencies in data through self-attention. For an image token, we compute Query (Q) $\rightarrow$ what am I looking for?, Key (K) $\rightarrow$ what do I contain? and Value (V) $\rightarrow$ what information do I carry? We can compute this attention score as,

$$\text{Attention}(\mathbf{Q}, \mathbf{K}, \mathbf{V}) = \text{Softmax}(\frac{\mathbf{Q}\mathbf{K}^T}{\sqrt{d}})\mathbf{V}, \tag{1}$$

where d is the number of features in each key/query vector. Thus, now with attention, each token becomes a context-aware representation. In multihead attention, multiple attention heads are processed in parallel. In

PixNav, they use transformer decoder layers with masked multihead self-attention, thereby preventing the agent from peeking into future frames.

$$\text{MultiHead}(\mathbf{Q}, \mathbf{K}, \mathbf{V}) = \text{Concat}(head_1, ..., head_n)\mathbf{W}, \tag{2}$$

where $head_n$ is the nth attention head.

3.2.1 RGB-PixNav

This section describes our approach to reproducing the results from Cai et al. (2024) using our proposed PixNav Trajectories dataset. In RGB-PixNav, the agent solely relies on RGB goal descriptors and observations to predict the next best action. The agent is exposed to dataset $D = \{(x_1, y_1), (x_2, y_2), ...(x_n, y_n)\}$ where the sample $x_i = (goal\ image; goal\ mask; observation\ history)$ and the label $y_i = (action_i, distance_i, mask_i)$. Here, (x_i, y_i) corresponds to the data tuple of step i in a trajectory. In pixel navigation, the agent only sees pixel-level details as input. A goal mask is a binary 2D mask generated from the goal image that indicates the target's pixel coordinates. The ground-truth pixel is expanded to an 8×8 local neighbourhood centred on the target pixel, with all pixels within the window labelled as positive. The goal image and goal mask together serve as the goal descriptors. The agent also receives RGB observations from the environment at each time step. During each learning iteration, the model is given a batch of goal descriptors and a history of K RGB images from each trajectory. As mentioned in Cai et al. (2024), the goal descriptors are concatenated along the channel dimension and passed through the goal encoder network (4-channel Resnet-18 He et al. (2016)). The resultant embedding is average-pooled and projected to sizes 768 and 256 via linear layers as the goal input token and the goal concat token, respectively. The past K observations serve as a history to help the agent learn temporal representations from the data. For this, observation data is also passed through an observation encoder (Resnet-18) network. The resultant embedding is pooled and projected to 512 dimensions. The so-obtained features are passed through 4 layers of a transformer decoder with masked attention to ensure causality. The resultant embedding is a 768-dimensional vector and is passed to 3 MLP heads for action prediction, coordinate prediction, and distance estimation. The action prediction head ensures the model learns to predict actions closely like an Oracle agent (ground truth). The coordinate prediction head ensures the agent can keep track of the goal pixels during motion. The distance prediction head ensures the agent estimates the distance to the target. The architecture shown in Figure 1 represents the proposed RGBD PixNav policy. The same architecture without depth observation inputs can be referred to as the RGB-PixNav policy. Cai et al. (2024) proposed a multiobjective loss function for pixel navigation with three components to address three heads. Action loss $\mathcal{L}_{act}$ can be formally defined as the cross-entropy loss between the predicted actions p_{ij} and the corresponding ground truth y_{ij} for a sample of 64 steps.

$$\mathcal{L}_{\text{act}} = -\frac{1}{N}\sum_{i=1}^{N}\sum_{j=1}^{C} y_{ij}\log(p_{ij}). \tag{3}$$

Distance loss, $\mathcal{L}_{dist}$, is the Mean Squared Error (MSE) between the predicted and actual distances over K timesteps.

$$\mathcal{L}_{\text{dist}} = \frac{1}{K}\sum_{i=1}^{K}\left(\hat{d}_i - d_i\right)^2, \tag{4}$$

where $\hat{d}_i$ is the predicted distance at step i and d_i is the ground truth distance at step i. This equation computes the average squared error between the predicted and actual distances across all 64 steps. Similarly, tracking loss, $\mathcal{L}_{track}$, is the Mean Squared Error (MSE) between the mask constructed from the predicted coordinates and the ground truth goal map over K timesteps.

$$L_{\text{track}} = \frac{1}{K}\sum_{i=1}^{K}\left(\hat{\mathcal{M}}_i - \mathcal{M}_i\right)^2, \tag{5}$$

where $\hat{\mathcal{M}}_i$ is the mask reconstructed with predicted coordinates at step i and $\mathcal{M}_i$ is the ground truth (actual) mask at step i. The overall objective is formulated as in (6), to minimize the weighted combination of each loss terms (3)-(5),

$$\theta^* = \arg\min_{\theta} \mathbb{E}_{(x_i,y_i)\sim D}\big[\mathcal{L}_{\text{act}}(x_i, y_i) + 0.1 \cdot \mathcal{L}_{\text{dist}}(x_i, y_i) + \mathcal{L}_{\text{track}}(x_i, y_i)\big]. \tag{6}$$

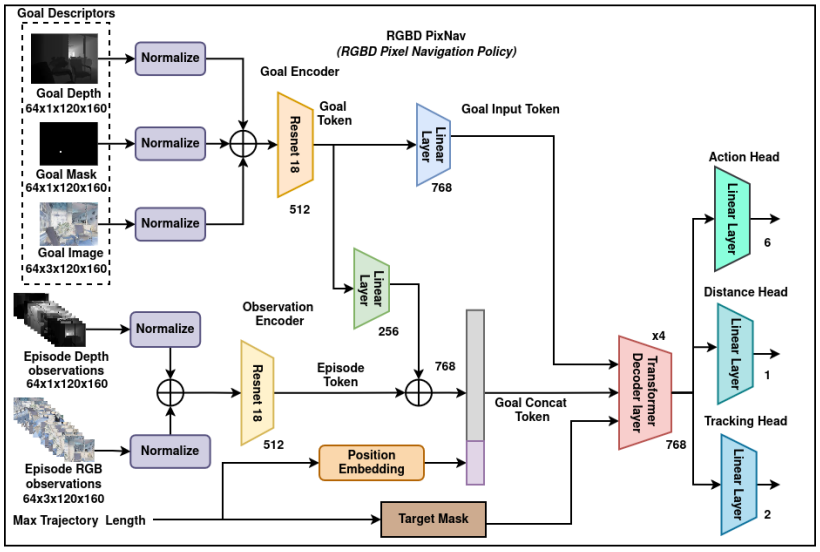

Figure 1: **Proposed architecture of RGBD-PixNav policy**. This architecture is a direct extension of Cai et al. (2024), here to introduce depth, the RGB and depth observations are concatenated along the channel dimension to goal and episode observation. In the case of RGB PixNav, episode depth observations are not considered.

3.2.2 RGBD-PixNav

In RGBD-PixNav, an embodied pixel navigation agent is built using RGB and depth modalities. Depth data is introduced to describe the goal and, at the observation level, to predict an action. The agent uses the dataset $D = \{(x_1, y_1), (x_2, y_2), ...(x_N, y_N)\}$ where the sample has $x_i = (goal\ image; goal\ mask; \textbf{goal depth map}; RGB\ observation\ history; \textbf{depth observation history})$ and $y_i = (action_i, distance_i, mask_i)$. Here, (x_i, y_i) corresponds to the data sample of step i in a trajectory. The goal mask is computed from the goal image as in 3.2.1, but here the goal depth map is also concatenated channel-wise with the input to the Goal Encoder. At each time step, the agent receives RGB and depth observations from the environment. Goal descriptors, a history of K RGB images, and K depth map observations are passed to the model as a sample. As mentioned in 3.2.1, the goal descriptors are concatenated along the channel dimension and passed through the goal encoder network (4-channel ResNet-18 He et al. (2016)); the resultant embedding is average-pooled to size 512 and projected to sizes 768 and 256 via linear layers. Similarly, the observation data is also passed through the observation encoder (a 3-channel ResNet-18 for RGB and a 1-channel ResNet-18 for depth). Observation embeddings are concatenated and projected to 512 dimensions. The goal token and fused observation feature with position embedding are passed through 4 layers of a transformer decoder to obtain the resultant vector, which is passed to 3 MLP heads for action prediction, coordinate prediction, and distance estimation. The same multiobjective loss function in section (3.2.1) with three components, corresponding to three heads, is reused here. The model objective can also be formulated as (6), as in RGB PixNav, where the dataset now contains RGBD samples.

3.3 Mamba-based Modeling for Pixel-guided Navigation

Mamba Gu & Dao (2024) is a lightweight, selective state space model (SSM) that operates with linear time complexity $O(T)$ and is specifically designed for sequence modeling. They have a strong inductive bias toward temporal modeling, making them a natural fit for navigation tasks. In navigation tasks, causality and temporal continuity matter more than pairwise attention. Vanilla SSMs, on the other hand, are input agnostic. A discrete-time linear SSM can be expressed as shown in (7).

$$\boldsymbol{s}_t = \mathbf{A}\boldsymbol{s}_{t-1} + \mathbf{B}\boldsymbol{u}_t \ , \ \boldsymbol{y}_t = \mathbf{C}\boldsymbol{s}_t, \tag{7}$$

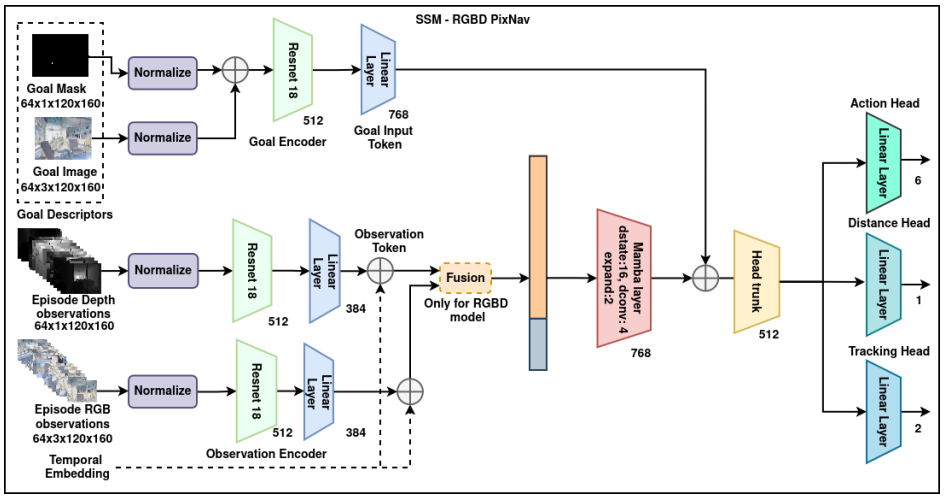

Figure 2: **Proposed architecture of SSM-based Pixel-guided Navigation**. The model is learnt end-to-end; the features from the goal descriptors and observations are fused after the temporal features are learned from the observations via a Mamba layer. Temporal embedding introduced ensures the ordering of the observation tokens.

where variable $\boldsymbol{s}_t \epsilon \mathbb{R}^N$ is the hidden state (memory), $\boldsymbol{u}_t \epsilon \mathbb{R}^D$ is the input and $\boldsymbol{y}_t \epsilon \mathbb{R}^D$ is the output. The matrices $\mathbf{A} \epsilon \mathbb{R}^{N \times N}$ is the state transition matrix (memory decay), $\mathbf{B} \epsilon \mathbb{R}^{N \times D}$ is the input projection matrix, and $\mathbf{C} \epsilon \mathbb{R}^{D \times N}$ is the readout matrix. N, D represent the state size and token embedding dimension, respectively. In SSM, with these matrices fixed, every input is treated equally. In Mamba, fixed dynamics are replaced with input-conditioned dynamics as shown in (8).

$$\boldsymbol{s}_t = \mathbf{A}(\boldsymbol{x}_t)\boldsymbol{s}_{t-1} + \mathbf{B}(\boldsymbol{x}_t)\boldsymbol{x}_t \ , \ \boldsymbol{y}_t = \mathbf{C}(\boldsymbol{x}_t)\boldsymbol{s}_t, \tag{8}$$

where $\boldsymbol{x}_t$ is the observation embedding and matrices $\mathbf{A}(\boldsymbol{x}_t)$, $\mathbf{B}(\boldsymbol{x}_t)$, $\mathbf{C}(\boldsymbol{x}_t)$ are learned functions of input. This, in turn, enables selective information propagation. In our proposed approaches, Mamba layers effectively capture sequential dependencies in observations through state-space modelling, unlike the transformer, which uses multi-head attention.

3.3.1 SSM-RGB PixNav Model

In this section, we propose a PixNav model trained with Mamba SSM layers. The proposed architecture is depicted in Figure 2 without depth inputs. In SSM-RGB PixNav, an embodied pixel navigation agent is built solely on the RGB modality. So, during training, the agent uses the dataset D with samples as defined in section 3.2.1. Goal image and goal mask, generated as in 3.2.1, serve as the goal descriptors. The agent also receives RGB observations from the environment at each time step. Goal descriptors and a history of K RGB image observations are passed to the model. The goal descriptors are then projected to a goal token of dimension 768 through a linear layer to match the Mamba layer dimension. The observation data is also passed through the observation encoder (Resnet 18) network. The embeddings from each frame are pooled and projected to 384 dimensions. These observation tokens are passed to the Mamba layer. The encoders help learn a better spatial representation, whereas the Mamba layers help with temporal modelling. The result from the Mamba layer is concatenated to the Goal token. The features are passed through a head trunk layer composed of a sequential layer with layernorm, a linear layer, ReLU, and dropout with a rate of 0.1. The resultant head-trunk feature of 512 dimensions is passed through 3 heads to predict the action, the coordinates, and the distance to the goal.

Temporal embedding ensures temporal ordering, but to ensure strict causality, a causal variant of the policy is proposed as shown in Figure 3. It introduces a mask that is 0 for future time steps and 1 for current and prior time steps. With the new mask, the input to the model now becomes $x_i = (goal\ image; goal\ mask; observation\ history;\ mask)$. Thus, by multiplying the mask with the history tokens, Mamba is ensured to see only the data up to T timesteps. Here, we combine the goal token

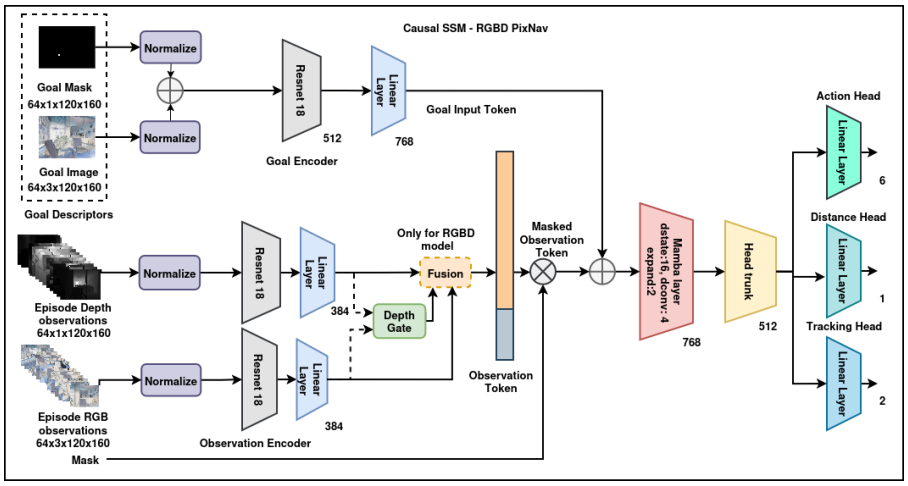

Figure 3: **Proposed architecture of Causal SSM-RGBD PixNav with depth gate**. In the case of Causal SSM-RGBD, Pixnav learned observation representations from the RGB and depth encoders, which are fused by concatenation. The fused embedding is multiplied by the mask and combined with the goal tokens. The goal-conditioned temporal features from the Mamba layer are passed through the trunk layer and the MLP heads. Whereas in Causal SSM-RGBD PixNav with depth-gate, an additional depth gate is added to learn the mixing ratio between the RGB and Depth features.

before passing it to the Mamba layer. Representation from the Mamba layer is passed through the head trunk layer and 3 prediction heads. This variant of the model is referred to as Causal SSM-RGB PixNav.

3.3.2 SSM-RGBD PixNav Model

Given the success of the depth extension of RGB PixNav, extending SSM-RGB PixNav with a depth modality is a natural next step. In SSM-RGBD PixNav, an embodied pixel navigation agent is built using RGB and depth modality inputs, leveraging the proposed architecture, as depicted in Figure 2. The agent uses the dataset D described in section (3.2.2). Goal image and goal mask, as in 3.2.1, serve as the goal descriptors. The K RGB and depth observations act as history to help the agent understand temporal cues. The observation data is passed through the observation encoders (a 3-channel Resnet-18 for RGB and a 1-channel Resnet-18 for Depth). The resultant embedding is projected to 384 dimensions. The same is separately embedded in time for ordering, then fused by concatenation. This fused feature is passed through Mamba layers to get a 768-dimensional vector. The resultant embedding is combined with the goal token and passed through the head trunk, yielding a 512-dimensional feature vector. The resultant vector is passed to 3 MLP heads for action prediction, coordinate prediction, and distance estimation. The same multiobjective loss function from (3.2.1) with three components, corresponding to three heads, is used.

For a causal variant, a mask is introduced at the input level as in Causal SSM-RGB Pixnav shown in Figure 3 and mixed with the fused observation token before being passed to the Mamba layer. This ensures the Mamba attends only to observations from previous time steps. In this variant of the RGBD model, features are fused via concatenation, allowing the agent to consider depth data even when it is noisy. To control this dependence on depth at every time step, a depth gate is introduced to learn when to rely on depth data, by analyzing observation data as shown in Figure 3. The learned mixing ratio is scaled to 50% to ensure the RGB is the dominant feature. With the learned mixing ratio, the representations are mixed and later masked for causality. The fused representation is combined with a goal token for goal conditioning and later passed through the Mamba layer. The agent now understands when to look at depth data and which fraction is important. With depth gating, masking, and early goal conditioning, the agent can make better predictions.

$$token_{depth} = 0.5 * \text{Sigmoid}(\text{Linear}(\text{Concat}(token_{rgb}, token_{depth}))) * token_{depth} \tag{9}$$

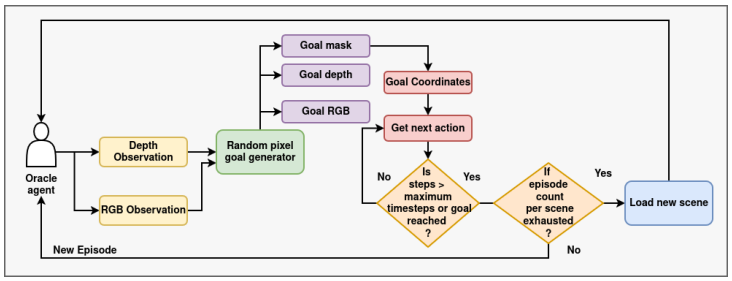

Figure 4: **Dataset generation pipeline** used to generate PixNav Trajectories dataset.

4 PixNav Trajectories Dataset

The dataset created for training pixel navigation through imitation learning, as part of Cai et al. (2024), was not publicly released. To address this lacuna, following the descriptions in the prior work closely, we have curated a dataset of navigation trajectories generated by the SPF oracle agent. Dataset curation and rollout validation of trained pixel navigation policies were done in Habitat-sim Savva et al. (2019),Szot et al. (2021),Puig et al.. Datasets comprising trajectories of maximum length $K = 64$ steps are used for training and evaluating the agent's policy. During data generation, as shown in Figure 4, in an episode, we first try to identify feasible random goal points in the scene. To this end, the depth data is projected to a point cloud format and tied with RGB pixels. A point is now randomly selected to ensure it is reachable. By doing so, we introduce randomness in the data itself. Despite numerous efforts, we were unable to reproduce the results reported in prior work due to random noise in the data. Following a supervised setting, the Shortest Path Follower (oracle agent) was used in the Habitat-sim to generate the ground truth. While collecting the data, the agent is initialized with the following settings: maximum step count of 64, a camera field of view of 79 degrees, and a camera height of 0.88m. The agent is made to navigate through 300,000 episodes. The agent skips the episode if the selected goal points proposed are not valid in an episode. If a valid goal is identified, the agent records it as a dataset sample. As depth data is freely available for an agent in Habitat-sim using the HM3D dataset, we have also curated depth maps for the RGBD model in the PixNav Trajectories dataset. In a trajectory, we have a goal described by an RGB goal image, a binary goal mask, and a depth map. Corresponding to each step in the trajectory, we have an RGB observation image, a binary goal mask tracked by the oracle agent, and a depth map, with remaining steps recorded as distances and the action taken by the oracle agent. Table 2 lists the different difficulty levels' definitions considered in the trajectories covered in the dataset. Policy rollout validation is done online. We relied on the SPF agent to obtain ground truth data, which achieved a success rate of 91.87%, 93.10% and 57.14% on easy, medium and hard episodes respectively on the rollout evaluation on HM3D dataset with Oracle Success Rate as a metric of dataset quality Wang et al. (2019).

Table 2: Distribution of train and validation splits by difficulty level.

Difficulty Level	Train Sample	Val Sample	Definition
Easy	34555	3445	Distance to goal is less than 3m.
Medium	33673	3430	Distance to goal is between 3 and 5m.
Hard	32016	3058	Distance to goal is between 5 and 8m.

5 Results

5.1 Pixel Navigation Rollout Validation

During training, after the model converges, we perform rollout validation on a few epochs from the region of convergence. During rollout validation, the agent is randomly initialized in the scene, and a random pixel goal is selected via point cloud projection and feasibility checks. The agent is now tested for its capability to reach the goal within the maximum allowed steps. As the trained agents move according to their own

Table 3: Pixel navigation policy evaluation results in the HM3D datasets. *This weight is shared by the authors of Cai et al. (2024) and is trained on a private dataset. All training was done with image resolution 120×160 following the training setup shared by Cai et al. (2024).

	Image	Model	Easy		Medium		Hard	
Model	**Size**	**Size**	**SR (↑)**	**SPL (↑)**	**SR (↑)**	**SPL (↑)**	**SR (↑)**	**SPL (↑)**
RGB PixNav *Cai et al. (2024)	224×224	54.449M	0.7497	0.7238	0.3448	0.3339	0.0476	0.0476
RGB PixNav *Cai et al. (2024)	120×160	54.449M	0.3123	0.2925	0.0345	0.0345	0.0476	0.0476
Ensemble (RGB + Depth) Krishnan R & etal (2026)	120×160	109.39M	0.4610	0.4304	0.0625	0.0625	0.1818	0.1818
RGB PixNav (baseline)	120×160	54.449M	0.3676	0.3441	0.1739	0.1726	0.1429	0.1429
SSM-RGB PixNav	120×160	27.624M	0.7545	0.7417	0.3091	0.3049	0.2000	0.2000
Causal SSM-RGB PixNav	120×160	**27.314M**	**0.8043**	**0.7905**	**0.4808**	**0.4727**	**0.2273**	**0.2273**
RGBD PixNav	120×160	54.455M	0.5361	0.4970	0.3800	0.3571	0.1500	0.1500
SSM-RGBD PixNav with Mamba	120×160	38.534M	0.5736	0.5350	0.3111	0.2987	0.2000	0.1980
Causal SSM-RGBD PixNav	120×160	38.780M	0.6894	0.6670	0.3200	0.3160	**0.3000**	**0.3000**
Causal SSM-RGBD PixNav with depth gate	120×160	**38.485M**	**0.7187**	**0.6934**	**0.4615**	**0.4520**	0.2727	0.2727

predictions, they start to deviate from the oracle agent's path, and the error begins to accumulate. This error accumulates over time as the agent tries to reach the goal. The trained policies are validated on HM3D Ramakrishnan et al. (2021) via rollout validation over 1000 episodes. Success Rate (SR) and Success Weighted Path Length (SPL) are the metrics identified to report the performance. A traversal is considered successful if and only if the distance to the goal at the end is $\leq$ 1m. The results obtained are tabulated in Table 3. From the numbers, we can see that the Causal SSM-RGB PixNav outperforms all the other models, and the Causal SSM-RGBD PixNav with a depth gate follows. More details on need for causal variant and role of depth gate are further explained in A.9 and A.10 respectively. The proposed models with the Mamba layer achieve remarkable gains in navigation metrics.

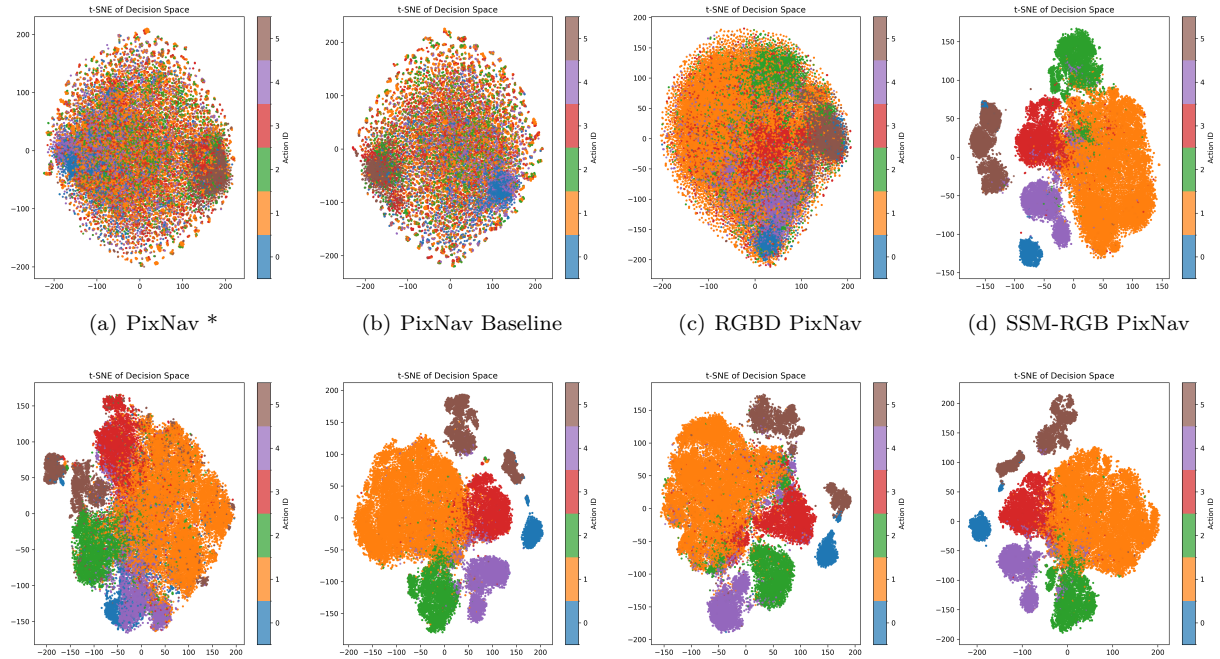

(a) PixNav *

(b) PixNav Baseline

(c) RGBD PixNav

(d) SSM-RGB PixNav

(e) Causal SSM-RGB PixNav

(f) SSM-RGBD PixNav

(g) Causal SSM-RGBD PixNav

(h) Causal SSM-RGBD PixNav with depth gate

Figure 5: **t-SNE plots of the representations learned** by all trained models from the validation trajectories in the PixNav Trajectories dataset. Subfigure (c) shows that introducing depth improves decision-making, whereas (d)-(h) have better separation, showing that Mamba is able to learn the goal-conditioned dynamics better. Labels 0 to 5 represent the 6 valid actions.* indicates weights from prior work Cai et al. (2024)

t-SNE plots are a means to visualize the separability of the learned representations. Through t-SNE, high-dimensional features can be projected to a lower-dimensional space in a supervised manner. To assess the models' ability to separate actions, t-SNE plots are generated from the validation fold data in the PixNav Trajectories dataset. The plots show better feature separability with Mamba-based models, which validate the numbers in Table 3. We attribute this to the Mamba model's ability to better capture data dynamics. As an ablation, a variant of the Causal SSM-RGB PixNav model was trained without the Mamba layers and with LSTM to learn the contribution of the Mamba layers. Results are discussed in A.5. Tracking capability is an important factor that helps the agent navigate to a pixel goal. The tracking performance of the best RGB and RGBD models during rollout evaluation from different time stamps is depicted in Figure 6. In Causal SSM-RGB PixNav, the goal in the next room is more closely tracked, whereas in Causal SSM-RGBD PixNav with depth gate, the agent at times gets confused by similar regions in the frame.
Since contributions to pixel navigation are limited, we compare our proposed models to those of the closely related task of goal instance navigation. Metrics reported in Table 9 from the HM3D dataset show that our proposed SSM-based policy achieves a higher SPL, indicating near-optimal trajectories in successful cases.

Figure 6: **Goal pixel tracking capability** of (a) Causal SSM-RGB PixNav, (b) Causal SSM-RGBD PixNav with depth gate is shown for random pixel goals in HM3D scenes. Pixel goal (red) and predicted goal coordinate (green) during rollout validation for episode images at different timesteps. It is clear that the Causal SSM-RGB PixNav model tracks the goal pixel more consistently. As depth gate regulates geometric cues, tracking relies primarily on appearance-based feature continuity. Additionally, temporal feature modulation introduced by depth gating might have slightly affected the stability of the representations passed to the Mamba layer.

5.2 Cross Dataset Validation

This experiment evaluates the generalization capability of pixel-guided navigation policies trained on the proposed PixNav Trajectories dataset, which is curated from the HM3D dataset. The dataset selected for

Table 4: Cross-dataset rollout evaluation of Pixel navigation policy on MP3D dataset.

	Image	Easy		Medium		Hard	
Model	**Size**	**SR (↑)**	**SPL (↑)**	**SR (↑)**	**SPL (↑)**	**SR (↑)**	**SPL (↑)**
RGB PixNav (baseline)	120 × 160	0.3542	0.3335	0.0510	0.0505	0.0909	0.0909
SSM-RGB PixNav	120 × 160	**0.6431**	**0.6327**	.1735	0.1713	**0.1212**	**0.1212**
Causal SSM-RGB PixNav	120 × 160	0.6418	0.6277	**0.2128**	**0.2090**	0.0968	0.0968
RGBD PixNav	120 × 160	0.3595	0.3400	0.1020	0.0979	0.0606	0.0606
SSM-RGBD PixNav	120 × 160	0.4234	0.3975	0.2121	0.2030	0.0667	0.0667
Causal SSM-RGBD PixNav	120 × 160	0.6117	**0.5964**	**0.2292**	**0.2244**	**0.1667**	**0.1667**
Causal SSM-RGBD PixNav with depth gate	120 × 160	**0.6183**	0.5963	0.2021	0.1992	0.0645	0.0645

cross-dataset evaluation is the MP3D dataset Chang et al. (2017). The rollout evaluation is also conducted with the same camera settings across 1000 episodes from the validation fold of the MP3D dataset. The numbers from Table 4 depict that the models trained on HM3D scenes are able to generalize to pixel-guided navigation problems in MP3D scenes. Mamba-based models still exhibit improved performance over the baseline, as seen in Table 3.

5.3 Robustness to Perturbation

In practice, all robots are prone to slight stability issues while navigating, which, in turn, affects the quality of the captured image frame and, eventually, the quality of the inferred features. To this end, an experiment was conducted on the trained model by perturbing the RGB and depth observation with additive Gaussian noise of varying standard deviation. The results obtained from all PixNav models for this experiment are tabulated in Table 5. The RGB PixNav model is the least robust to observation noise. As the noise increases, we can see the metrics drop significantly, especially in medium and hard cases. With SSM-based models, we can see that they perform consistently and the metrics degrade more gracefully. In RGBD variants, depth serves as a geometric prior; however, when the depth signal is noisy, the model becomes more sensitive to perturbations, as expected, due to degraded geometric cues. Causal variants with higher performance provide stronger temporal filtering and greater noise resilience.

Table 5: Robustness of proposed PixNav policies towards Gaussian Noise of mean zero.

	Standard	**Easy**		**Medium**		**Hard**	
Model	**Deviation**	**SR (↑)**	**SPL (↑)**	**SR (↑)**	**SPL (↑)**	**SR (↑)**	**SPL (↑)**
	0.02	0.1005	0.0853	0.0000	0.0000	0.0500	0.0500
PixNav*	0.03	0.0916	0.0774	0.0192	0.0163	0.1364	0.1364
(Author's weights	0.04	0.1038	0.0839	0.0189	0.0189	0.0800	0.0800
from Cai et al. (2024))	0.05	0.1110	0.0945	0.0000	0.0000	0.0769	0.0769
	0.02	0.3643	0.3398	0.1500	0.1478	0.1176	0.1176
RGB-PixNav	0.03	0.3501	0.3288	0.0833	0.0833	0.2400	0.2400
(baseline)	0.04	0.3470	0.3273	0.1250	0.1224	0.1579	0.1579
	0.05	0.3530	0.3326	0.0784	0.0784	0.2500	0.2500
	0.02	0.7459	0.7350	0.4681	0.4661	0.1739	0.1739
SSM-RGB PixNav	0.03	0.7076	0.6982	0.2500	0.2481	0.0000	0.0000
	0.04	0.6843	0.6750	0.2807	0.2803	0.0000	0.0000
	0.05	0.6507	0.6391	0.3000	0.3000	0.0870	0.0870
	0.02	**0.7596**	**0.7466**	**0.3600**	**0.3505**	**0.1852**	**0.1852**
Causal SSM-RGB PixNav	0.03	0.7595	0.7442	0.2727	0.2671	0.0952	0.0952
	0.05	0.7051	0.6909	0.2679	0.2624	0.1562	0.1562
	0.02	0.2674	0.2297	0.1026	0.1026	0.0000	0.0000
RGBD-PixNav	0.03	0.3084	0.2536	0.0357	0.0357	0.0000	0.0000
	0.04	0.2331	0.1941	0.0000	0.0000	0.0000	0.0000
	0.05	0.2072	0.1804	0.0851	0.0851	0.0000	0.0000
	0.02	0.4213	0.3838	0.1702	0.1629	0.1200	0.1200
SSM-RGBD PixNav	0.03	0.3939	0.3624	0.1509	0.1509	0.0455	0.0455
	0.04	0.4262	0.3863	0.1667	0.1572	.0833	0.0833
	0.05	0.4246	0.3874	0.1702	0.1682	0.0400	0.0400
	0.02	0.6750	0.6519	0.1875	0.1806	**0.1538**	**0.1538**
Causal SSM-RGBD PixNav	0.03	0.6446	0.6254	0.2830	0.2762	0.2222	0.2222
	0.04	0.6317	0.6129	0.2364	0.2348	0.2609	0.2609
	0.05	0.6178	0.5988	0.1136	0.1136	0.1739	0.1739
	0.02	**0.7092**	**0.6860**	**0.2500**	**0.2413**	0.0690	0.0690
Causal SSM-RGBD PixNav	0.03	0.6494	0.6323	0.2444	0.2356	0.1579	0.1579
with Depth gate	0.04	0.6093	0.5901	0.3061	0.2996	0.0625	0.0625
	0.05	0.6071	0.5888	0.3191	0.3148	0.1429	0.1429

6 Discussion

In this work, we first aim to establish a reproducible baseline for PixNav using only the RGB modality. We then added depth modality as a clear extension by concatenating depth data along the channel dimension. This simple step led to a large gain in the success rate of ≈ 0.1685 on the easy episodes. The behaviour is consistent across episodes of varying complexity and datasets. However, the computational complexity of these models is of $O(N^2)$, and therefore, we looked for a lighter variant of the solution. In the SSM-based models, Mamba layers were incorporated to capture the dynamics in the observation features. We proposed a lighter model $\approx 27M$ with a significant performance gain of ≈ 0.39 on the easy episodes. Temporal ordering is already handled, but to ensure causality, a mask was introduced, boosting performance by ≈ 0.44 on easy episodes relative to the baseline. Training setup and hypermeter used for each variant is briefed in A.1

Why could Mamba have helped? To understand this part more closely, at each time step t, latent state $\boldsymbol{h}_t$ can be defined in terms of input-dependent state matrices $\mathbf{A}$ and $\mathbf{B}$ as,

$$\boldsymbol{h}_t = \bar{\mathbf{A}}_t \boldsymbol{h}_{t-1} + \bar{\mathbf{B}}_t \boldsymbol{x}_t, \tag{10}$$

where $\bar{\mathbf{A}}_t$ is the transition matrix and $\bar{\mathbf{B}}_t$ is the input projection matrix. Unrolling the recurrence gives,

$$\boldsymbol{h}_t = \sum_{k=1}^{t} \left(\prod_{j=k+1}^{t} \bar{\mathbf{A}}_j \right) \bar{\mathbf{B}}_k \boldsymbol{x}_k, \tag{11}$$

which shows that the latent state aggregates past observations through a sequence of learned, time-varying transition operators. Goal conditioning is introduced as an additive latent bias $\boldsymbol{g}$, resulting in,

$$\hat{\boldsymbol{h}}_t = \boldsymbol{h}_t + \boldsymbol{g} = \sum_{k=1}^{t} \mathbf{K}_{t,k} \boldsymbol{x}_k + \boldsymbol{g}, \tag{12}$$

where $\mathbf{K}_{t,k} = (\prod_{j=k+1}^{t} \bar{\mathbf{A}}_j)\bar{\mathbf{B}}_k$. This formulation allows the policy to reason about observations relative to the target in a goal-shifted latent space, without explicitly modifying the underlying dynamics. Even though RGBD SSM-PixNav's performance is slightly lower than SSM-PixNav, the model remains competent and its performance is better than the transformer-based approach. As an ablation study, we have varied K, the number of history frames during rollout evaluation, to see how many history frames the model actually leverages. More details of the experiment can be seen in A.3. The results show that higher K yields better temporal features. Similarly, an experiment was conducted to evaluate the model's zero-shot object goal

Table 6: **Sensitivity Analysis.** Results from rollout evaluation of agent on HM3D dataset by varying K, the number of history frames.

		Easy		Medium		Hard	
Model	K	**SR** (↑)	**SPL** (↑)	**SR** (↑)	**SPL** (↑)	**SR** (↑)	**SPL** (↑)
Causal SSM-RGB PixNav	4	0.3625	0.3322	0.0727	0.0697	0.2000	0.2000
	8	0.5982	0.5739	0.3061	0.2968	0.0455	0.0455
	16	0.7957	0.7834	0.2195	0.2091	0.1053	0.1053
	32	**0.8043**	**0.7906**	**0.5000**	**0.4920**	**0.2273**	**0.2273**
Causal SSM-RGBD PixNav with gate	4	0.4023	0.3749	0.0909	0.0857	0.0000	0.0000
	8	0.5497	0.5241	0.2449	0.2285	0.0909	0.0909
	16	0.7049	0.6833	0.2439	0.2318	0.1579	0.1579
	32	**0.7187**	**0.6934**	**0.4615**	**0.4520**	**0.2727**	**0.2727**

navigation capability, leveraging guidance from an open-source VLM. The details of the same are given in (A.7). The results show that the SSM models perform slightly better than the author's weights Cai et al. (2024). While testing the models on NVIDIA AGX Orin with the OAK-D Pro camera, it was noted that the mean time to predict an action for SSM models is reduced by 10-15ms compared to the transformer-based variants. SSM variants show higher speed-up in inferencing on edge compute, with the Causal SSM-RGB PixNav model reaching 17%, which is crucial for mobile agents. More details of this experiment can be found in (A.8).

7 Conclusions

This work addresses the pixel-guided navigation problem, traditionally approached using only RGB inputs in embodied navigation, by extending the modeling framework to incorporate available depth information via RGBD-PixNav. The incorporation of depth maps allows the agent to leverage additional geometric cues, enhancing navigation performance in visually complex environments. To address the lack of an open-source dataset for supervised training of pixel navigation policies, a new benchmark dataset was curated for this effort. Toward better temporal modelling, Mamba layers were introduced. With changes in the goal-fusion strategy, the proposed SSM-based models were developed to clarify what to focus on.

Experimental results demonstrate that the proposed models, Causal SSM RGB PixNav followed by Causal SSM RGBD PixNav with depth gate, consistently outperform the RGB-only baseline and other proposed policy variants in pixel navigation tasks. The proposed policies also exhibit robust behaviour to mild Gaussian noise and variations in history frames. Proposed Causal SSM-RGB PixNav achieved a speed up in inference time of 17% on edge compute. The current approach relies on supervised learning, and the agent is exposed predominantly to clean expert data. Future directions include incorporating Dagger-based fine-tuning or other strategies to improve policy robustness in more realistic scenarios and addressing the sim-to-real gap.

References

Peter Anderson, Angel X. Chang, Devendra Singh Chaplot, Alexey Dosovitskiy, Saurabh Gupta, Vladlen Koltun, Jana Kosecka, Jitendra Malik, Roozbeh Mottaghi, Manolis Savva, and Amir R. Zamir. On evaluation of embodied navigation agents. *CoRR*, abs/1807.06757, 2018. URL `http://arxiv.org/abs/1807.06757`.

Lucas Beyer, Andreas Steiner, André Susano Pinto, Alexander Kolesnikov, Xiao Wang, Daniel Salz, Maxim Neumann, Ibrahim Alabdulmohsin, Michael Tschannen, Emanuele Bugliarello, et al. Paligemma: A versatile 3b vlm for transfer. *arXiv preprint arXiv:2407.07726*, 2024.

Wenzhe Cai, Siyuan Huang, Guangran Cheng, Yuxing Long, Peng Gao, Changyin Sun, and Hao Dong. Bridging zero-shot object navigation and foundation models through pixel-guided navigation skill. In *2024 IEEE International Conference on Robotics and Automation (ICRA)*, pp. 5228–5234. IEEE, 2024.

Angel Chang, Angela Dai, Thomas Funkhouser, Maciej Halber, Matthias Niessner, Manolis Savva, Shuran Song, Andy Zeng, and Yinda Zhang. Matterport3D: Learning from RGB-D data in indoor environments. *International Conference on 3D Vision (3DV)*, 2017.

Devendra Singh Chaplot, Dhiraj Prakashchand Gandhi, Abhinav Gupta, and Russ R Salakhutdinov. Object goal navigation using goal-oriented semantic exploration. *Advances in Neural Information Processing Systems*, 33:4247–4258, 2020.

Arnab Debnath, Gregory J. Stein, and Jana Kosecka. Semnav: A model-based planner for zero-shot object goal navigation using vision-foundation models. In *Workshop on Foundation Models Meet Embodied Agents at CVPR 2025*, 2025. URL `https://openreview.net/forum?id=EZlJLnyI8L`.

Albert Gu and Tri Dao. Mamba: Linear-time sequence modeling with selective state spaces. In *First conference on language modeling*, 2024.

Kaiming He, Xiangyu Zhang, Shaoqing Ren, and Jian Sun. Deep residual learning for image recognition. In *Proceedings of the IEEE conference on computer vision and pattern recognition*, pp. 770–778, 2016.

Chenguang Huang, Oier Mees, Andy Zeng, and Wolfram Burgard. Audio visual language maps for robot navigation. In *International Symposium on Experimental Robotics*, pp. 105–117. Springer, 2023a.

Chenguang Huang, Oier Mees, Andy Zeng, and Wolfram Burgard. Visual language maps for robot navigation. In *2023 IEEE International Conference on Robotics and Automation (ICRA)*, pp. 10608–10615. IEEE, 2023b.

Alexander Kirillov, Eric Mintun, Nikhila Ravi, Hanzi Mao, Chloe Rolland, Laura Gustafson, Tete Xiao, Spencer Whitehead, Alexander C Berg, Wan-Yen Lo, et al. Segment anything. In *Proceedings of the IEEE/CVF international conference on computer vision*, pp. 4015–4026, 2023.

Athira Krishnan R and etal. Tepen: Towards an ensemble model for pixel-based embodied navigation. In Sushmita Mitra, Sriparna Saha, Bijaya Ketan Panigrahi, Sudeep Sarkar, and Santanu Chaudhury (eds.), *Pattern Recognition and Machine Intelligence*, pp. 60–67, Cham, 2026. Springer Nature Switzerland. ISBN 978-3-032-18477-1.

Junnan Li, Dongxu Li, Caiming Xiong, and Steven Hoi. Blip: Bootstrapping language-image pre-training for unified vision-language understanding and generation. In *International conference on machine learning*, pp. 12888–12900. PMLR, 2022.

Shilong Liu, Zhaoyang Zeng, Tianhe Ren, Feng Li, Hao Zhang, Jie Yang, Qing Jiang, Chunyuan Li, Jianwei Yang, Hang Su, et al. Grounding dino: Marrying dino with grounded pre-training for open-set object detection. In *European conference on computer vision*, pp. 38–55. Springer, 2024.

Arjun Majumdar, Gunjan Aggarwal, Bhavika Devnani, Judy Hoffman, and Dhruv Batra. Zson: Zero-shot object-goal navigation using multimodal goal embeddings. In S. Koyejo, S. Mohamed, A. Agarwal, D. Belgrave, K. Cho, and A. Oh (eds.), *Advances in Neural Information Processing Systems*, volume 35, pp. 32340–32352. Curran Associates, Inc., 2022. URL https://proceedings.neurips.cc/paper_files/paper/2022/file/d0b8f0c8f79d3a621af945cafb669f4b-Paper-Conference.pdf.

Joakim Niklasson, Sofia Backåberg, Terese Lindberg, Patrick Bergman, and Cecilia Fagerström. Embodied navigation: the influence of lived experience on physical activity and sedentary behavior among older adults. *International Journal of Qualitative Studies on Health and Well-being*, 19(1):2313657, 2024. doi: 10.1080/17482631.2024.2313657. URL https://doi.org/10.1080/17482631.2024.2313657. PMID: 38349928.

OpenAI. Gpt-4 technical report, 2023. URL https://openai.com/research/gpt-4. Accessed: 2025-07-18.

Xavier Puig, Eric Undersander, Andrew Szot, Mikael Dallaire Cote, Tsung-Yen Yang, Ruslan Partsey, Ruta Desai, Alexander William Clegg, Michal Hlavac, So Yeon Min, et al. Habitat 3.0: A co-habitat for humans, avatars and robots, 2023. *URL https://arxiv. org/abs/2310.13724*.

Alec Radford, Jong Wook Kim, Chris Hallacy, Aditya Ramesh, Gabriel Goh, Sandhini Agarwal, Girish Sastry, Amanda Askell, Pamela Mishkin, Jack Clark, et al. Learning transferable visual models from natural language supervision. In *International conference on machine learning*, pp. 8748–8763. PmLR, 2021.

Santhosh Kumar Ramakrishnan, Aaron Gokaslan, Erik Wijmans, Oleksandr Maksymets, Alexander Clegg, John Turner, Eric Undersander, Wojciech Galuba, Andrew Westbury, Angel Chang, Manolis Savva, Yili Zhao, and Dhruv Batra. Habitat-matterport 3d dataset (hm3d): 1000 large-scale 3d environments for embodied ai. In J. Vanschoren and S. Yeung (eds.), *Proceedings of the Neural Information Processing Systems Track on Datasets and Benchmarks*, volume 1, 2021. URL https://datasets-benchmarks-proceedings.neurips.cc/paper_files/paper/2021/file/34173cb38f07f89ddbebc2ac9128303f-Paper-round2.pdf.

Manolis Savva, Abhishek Kadian, Oleksandr Maksymets, Yili Zhao, Erik Wijmans, Bhavana Jain, Julian Straub, Jia Liu, Vladlen Koltun, Jitendra Malik, et al. Habitat: A platform for embodied ai research. In *Proceedings of the IEEE/CVF international conference on computer vision*, pp. 9339–9347, 2019.

Jingwen Sun, Jing Wu, Ze Ji, and Yu-Kun Lai. A survey of object goal navigation. *IEEE Transactions on Automation Science and Engineering*, 22:2292–2308, 2024.

Andrew Szot, Alexander Clegg, Eric Undersander, Erik Wijmans, Yili Zhao, John Turner, Noah Maestre, Mustafa Mukadam, Devendra Singh Chaplot, Oleksandr Maksymets, Aaron Gokaslan, Vladimír Vondruš, Sameer Dharur, Franziska Meier, Wojciech Galuba, Angel Chang, Zsolt Kira, Vladlen Koltun, Jitendra Malik, Manolis Savva, and Dhruv Batra. Habitat 2.0: Training home assistants to rearrange their habitat. In M. Ranzato, A. Beygelzimer, Y. Dauphin, P.S. Liang, and J. Wortman Vaughan (eds.), *Advances in Neural Information Processing Systems*, volume 34, pp. 251–266. Curran Associates, Inc., 2021. URL https://proceedings.neurips.cc/paper_files/paper/2021/file/021bbc7ee20b71134d53e20206bd6feb-Paper.pdf.

Ashish Vaswani, Noam Shazeer, Niki Parmar, Jakob Uszkoreit, Llion Jones, Aidan N Gomez, Ł ukasz Kaiser, and Illia Polosukhin. Attention is all you need. In I. Guyon, U. Von Luxburg, S. Bengio, H. Wallach, R. Fergus, S. Vishwanathan, and R. Garnett (eds.), *Advances in Neural Information Processing Systems*, volume 30. Curran Associates, Inc., 2017. URL https://proceedings.neurips.cc/paper_files/paper/2017/file/3f5ee243547dee91fbd053c1c4a845aa-Paper.pdf.

Xin Wang, Qiuyuan Huang, Asli Celikyilmaz, Jianfeng Gao, Dinghan Shen, Yuan-Fang Wang, William Yang Wang, and Lei Zhang. Reinforced cross-modal matching and self-supervised imitation learning for vision-language navigation. In *Proceedings of the IEEE/CVF conference on computer vision and pattern recognition*, pp. 6629–6638, 2019.

Hang Yin, Xiuwei Xu, Linqing Zhao, Ziwei Wang, Jie Zhou, and Jiwen Lu. Unigoal: Towards universal zero-shot goal-oriented navigation. In *Proceedings of the IEEE/CVF Conference on Computer Vision and Pattern Recognition*, pp. 19057–19066, 2025.

Jiazhao Zhang, Kunyu Wang, Rongtao Xu, Gengze Zhou, Yicong Hong, Xiaomeng Fang, Qi Wu, Zhizheng Zhang, and He Wang. Navid: Video-based vlm plans the next step for vision-and-language navigation. *Robotics: Science and Systems*, 2024.

Jiazhao Zhang, Kunyu Wang, Shaoan Wang, Minghan Li, Haoran Liu, Songlin Wei, Zhongyuan Wang, Zhizheng Zhang, and He Wang. Uni-navid: A video-based vision-language-action model for unifying embodied navigation tasks. *Robotics: Science and Systems*, 2025.

Xinxin Zhao, Wenzhe Cai, Likun Tang, and Teng Wang. Imaginenav: Prompting vision-language models as embodied navigator through scene imagination. In *The Thirteenth International Conference on Learning Representations*.

Deyao Zhu, Jun Chen, Xiaoqian Shen, Xiang Li, and Mohamed Elhoseiny. Minigpt-4: Enhancing vision-language understanding with advanced large language models. In *The Twelfth International Conference on Learning Representations*, 2023.

A Appendix

A.1 Training setup

The models are trained on the proposed dataset. For training and evaluation, 100000 trajectories from the train fold and 10000 trajectories from the validation fold were used. All models were trained for 30 epochs. All fine-grained training details like learning rate, optimizer, scheduler are mentioned in Table 7 for reproducibility. The images were resized to 120x160 resolution and normalized. All transformer model

Table 7: Training set up used for the suite of pixel-guided navigation policies.

Model	Optimizer	Scheduler	Learning rate	Weight Decay
RGB PixNav	Adam	LR Scheduler	1e-5	1e-4
SSM - RGB PixNav	Adam	CosineAnnealingLR	1e-4	3e-4
Causal SSM - RGB PixNav with Mamba Causal	AdamW	ReduceLROnPlateau	1e-4	1e-4
RGBD PixNav	Adam	LR Scheduler	1e-5	1e-4
SSM - RGBD PixNav	AdamW	CosineAnnealingLR	7e-5	1e-4
Causal SSM - RGBD PixNav	AdamW	CosineAnnealingLR	7e-5	1e-4
Causal SSM - RGBD PixNav with depth gate	AdamW	CosineAnnealingLR	7e-5	1e-4

training was done on a 64GB Mac Studio, and Mamba model training was done on a NVIDIA 5090. All rollout evaluations were conducted on an NVIDIA L40 machine.

A.2 Metrics

The efficiency of any model needs to be compared, but to compare them, we need some measuring aids. In DL, we term them as metrics. The metrics generally used for navigation domains Sun et al. (2024) include Success Rate, Success Weighted Path Length, Soft SPL, and Distance to Goal. Each metric and its formulation are briefly described in the subsections below.

A.2.1 Success Rate

Success Rate (SR) is the percentage of successful attempts of navigation an agent made to reach the goal. An agent is considered successful if it reaches within a goal radius of 1m. So mathematically the same can be framed as,

$$SR = \frac{1}{N}\sum_{i=1}^{N}\begin{cases}1, & \text{if success}\\ 0, & \text{else,}\end{cases} \tag{13}$$

where N is the number of episodes considered. As a successful agent aimed for, a higher SR is preferred.

A.2.2 Success Weighted Path Length

For a navigation agent, success is important, but the effort or path length taken to reach a goal is equally important. The longer the path length, the more energy will be required to navigate it. So, through Success Weighted Path Length (SPL) Anderson et al. (2018), a trade-off is established to weight successes and path length. Out of N episodes considered, in each episode, l_i is the length of the shortest/optimal path from the starting position of the agent to reach the goal. Similarly, p_i is the length of the path actually taken by the agent. Let S_i be the success, which takes the value 1 for success and 0 for failure. Now SPL can be mathematically defined as,

$$SPL \;=\; \frac{1}{N}\sum_{i=1}^{N} S_i \frac{l_i}{\max(l_i, p_i)}. \tag{14}$$

SPL takes a value of 0 if success is 0; otherwise, its value ranges from 0 to 1. A higher SPL is preferred because it means a shorter path length to the goal.

A.2.3 Soft SPL

Soft SPL (SSPL) is a softer version of SPL, which does not depend on the success factor. So, even if the attempt is unsuccessful, we can still implement this measure. For the same setting considered while defining SPL, SSPL can be defined as,

$$SPL \;=\; \frac{1}{N}\sum_{i=1}^{N} \frac{l_i}{\max(l_i, p_i)}. \tag{15}$$

A.2.4 Distance to Goal

Distance to goal (DTG) is measured once the agent issues a STOP action/maximum allowed number of steps is exhausted. In this stage, the geodesic distance from the agent's current position to the goal location is measured. As reaching closer to the goal increases the likelihood of success, a lower DTG is preferred.

A.3 Varying the number of history frames

Mamba has a selective-scanning property, so the model examines unique frames. The longer the history, the better the temporal insights the model learns. But how to validate that the higher the number of history frames considered, the better the navigation?
To this end, an ablation was performed at rollout validation by varying/ truncating the history observations to different ranges, $K = \{4, 8, 16, 32\}$. The experiment was conducted on the best-performing models from each RGB and RGBD variant to assess changes in performance. The results are tabulated in Table 6, which shows that as K decreases, knowledge about the environment is lost/truncated, leading to the representations learned. This directly affects the performance. The same trend is visible in both the variants tested, which revalidates that the higher the number of history frames considered, the better the temporal representations learned by the model. Another observation is that, in both cases, the performance with 32 frames is similar to that with 64 frames. This shows that the Mamba layer, through selective scan, attends to 32 frames even when we use 64 frames.

A.4 Robustness to Pertubation

The observation frames are perturbed with Gaussian noise. The mean of the noise is kept zero, but the standard deviation is varied from 2 to 5 percent. A sample observation image with different levels of noise injection is shown in Figure 7.

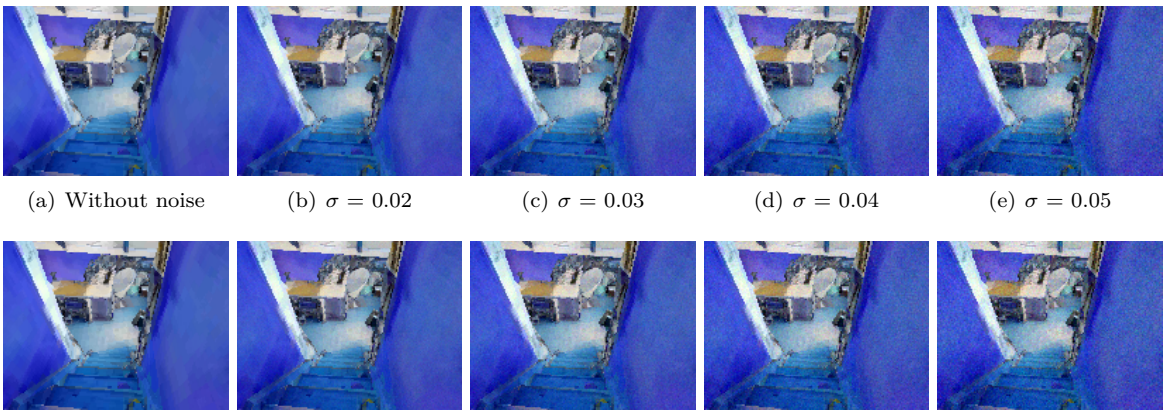

(a) Without noise (b) $\sigma = 0.02$ (c) $\sigma = 0.03$ (d) $\sigma = 0.04$ (e) $\sigma = 0.05$

(f) Without noise (g) $\sigma = 0.02$ (h) $\sigma = 0.03$ (i) $\sigma = 0.04$ (j) $\sigma = 0.05$

Figure 7: **Noise augmented episode observation**. Sample episode RGB observation and its noisy versions from a Gaussian of different standard deviations.

A.5 Effect of Mamba Layer

To assess the contribution of the Mamba layer in the proposed Causal SSM - RGB PixNav model, a variant was trained and evaluated without it. This model, with 22.952M parameters, takes the masked version of the fused encoded observation features and concatenates them with goal features. Here, because the model is less complex, the goal and observation features are projected to 384 dimensions. Rollout performance of the same is recorded in Table 8. Even the t-SNE plot shown in Figure 8 clearly depicts the lack of a Mamba-like efficient temporal modeling.

Table 8: Pixel navigation policy evaluation results in the HM3D datasets. The model used here is the same as the proposed Causal SSM-RGB PixNav, but Mamba layers are skipped.

Model	Dataset	Easy		Medium		Hard	
		SR (↑)	SPL (↑)	SR (↑)	SPL (↑)	SR (↑)	SPL (↑)
Causal SSM-RGB PixNav	HM3D	**0.8043**	**0.7905**	**0.4808**	**0.4727**	**0.2273**	**0.2273**
	MP3D	0.6418	0.6277	**0.2128**	**0.2090**	**0.0968**	**0.0968**
Causal SSM-RGB PixNav (w/o Mamba)	HM3D	0.2468	0.2373	0.0727	0.0727	0.1000	0.1000
	MP3D	0.0824	0.0807	0.0000	0.0000	0.0303	0.0303
Causal LSTM-RGB PixNav	HM3D	0.7764	0.7685	0.2826	0.2781	0.1500	0.1451
	MP3D	**0.6598**	**0.6484**	0.1700	0.1696	0.0800	0.0800

As an ablation, we have also tried replacing the Mamba layer in Causal SSM-RGB PixNav with an LSTM layer. After training under a similar setup, the policy was evaluated. The rollout evaluation metrics from Table 8 show that this 24.14M-parameter policy performs well on easy episodes ($\approx 3\% \downarrow$ compared to Causal SSM-RGB PixNav). But the performance drops substantially as the difficulty increases.

A.6 Goal Instance Navigation

In goal instance navigation, given a goal image and its goal category type, the agent is expected to move towards the goal. Even though in pixel navigation we do not consider the object type, but consider the pixel location, this is the most similar problem in research.

From the metrics, we can see that our lightweight standalone models achieve a competitive success rate compared to Unigoal Yin et al. (2025), which relies on VLMs to make decisions. But the most important observation is the substantially higher SPL in our trajectories. This ensures that our model can plan efficient trajectories, especially during successful detours.

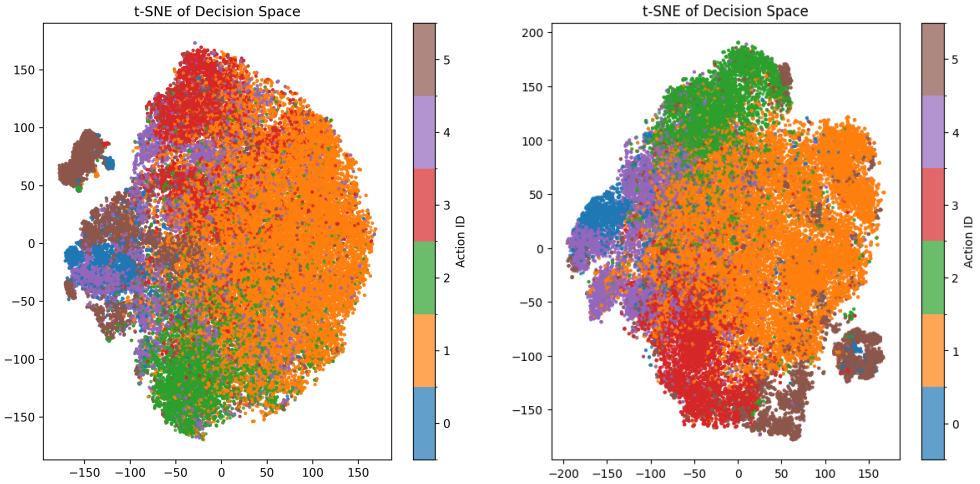

(a) Without Mamba Layer

(b) LSTM PixNav

Figure 8: **t-SNE plot for SSM-RGB PixNav model without Mamba layer and Causal LSTM-RGB PixNav model**. In the model without the Mamba layer, we observe that spatial features help to some extent, but feature separability is lower than that of the proposed SSM variants shown in Figure 5. LSTM variant shows better separability than one without Mamba layer, but not to the level of Causal SSM-RGB PixNav shown in Figure 5.

Table 9: **Metric from SOTA Goal Instance navigation models** on HM3D dataset from Yin et al. (2025). * indicates the metrics were taken from Yin et al. (2025) as the pre-trained weights or scripts to reproduce were missing. Metrics of Yin et al. (2025) are reported from 200 episodes from the HM3D dataset.

Task	Model	SR	SPL
Goal Instance navigation	OVRL-v2-IIN*	0.248	0.118
Goal Instance navigation	GOAT*	0.374	0.161
Goal Instance navigation	Unigoal	**0.68500**	0.25050
Pixel Navigation	Causal SSM-RGB PixNav	0.5041	**0.4968**
Pixel Navigation	Causal SSM-RGBD PixNav with depth gate	0.4843	0.4727

Table 10: **Zero-shot object goal navigation** results from Pix Nav models on 100 HM3D validation episodes.

Model	Resolution	SR (↑)	SPL (↑)	SSPL (↑)	Distance To Goal (↓)	Distance To Predicted Goal (↓)
PixNav*	120 × 160	9	0.0517	0.0961	5.894	1.3238
PixNav(baseline)	120 × 160	2	0.02	0.0730	5.585	0.8667
SSM-RGB PixNav	120 × 160	**9**	**0.0638**	**0.1129**	**5.826**	1.1713
Causal SSM-RGB PixNav	120 × 160	3	0.0233	0.0937	5.560	1.0742
RGBD PixNav	120 × 160	0	0	0.0011	5.627	0.8387
SSM-RGBD PixNav	120 × 160	0	0	0.0079	5.538	0.8202
Causal SSM-RGBD PixNav	120 × 160	0	0	0.0024	5.547	0.8202
Causal SSM-RGBD PixNav with depth gate	120 × 160	0	0	0.0061	5.566	0.8205

A.7 Zero-shot object goal navigation

This section aims to test the model's suitability for solving object-goal navigation. As the model lacks the capability to understand object type/text guidance, we propose a method that utilizes the foundation models Grounding DINO Liu et al. (2024) and SAM Kirillov et al. (2023). Here, the agent is initialized in an episode scene in Habitat using the HM3D dataset. For the object goal described in the dataset, the agent tries to complete object goal navigation.

Given an object goal, the agent first tries to determine the probable direction to explore to find the specified object. For example, a bed is found in the bedroom, a sink is found in the kitchen, and so on. To this end, the agent rotates by 360° and captures the observations. Considering the FOV as 90°, and there are 12 steps to reduce the overlap, every alternate observation is omitted to construct a panorama. The panorama is passed to a VLM to determine the probable direction. Now the agent turns in that direction and passes the observation to the object detector to detect the object in the frame. If the object is present, the current observation image serves as the goal image, and the SAM-generated mask serves as the goal mask for the pixel navigation agent. If the object is absent, the agent looks for the floor class. The observation and the SAM-generated mask are now passed to the pixel navigation agent. If the agent is stuck, it tries to capture the panorama and plan again. This loop of actions continues until the agent reaches the goal. An attempt is considered successful, iff the agent reaches within 1m proximity to the goal.

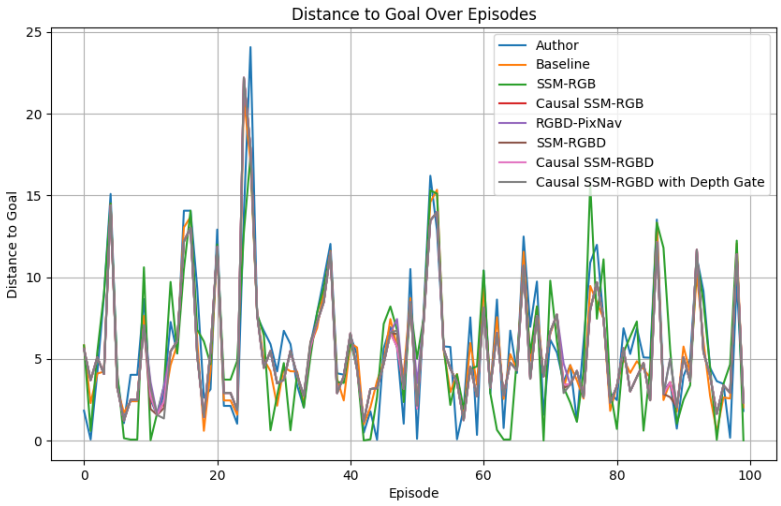

Figure 9: **DTG measures the closeness of the goal position to the stopping position**. The DTG of different models is shown here.

It is evident that performance has dropped with the BLIP planner. If the planner predicts the wrong direction, the agent tries to look for the object or floor category. It will go by floor category if the object is not visible. Being indoors, some floor space will be visible, which will mislead the agent in the wrong direction. This is expected to be a problem with our open-source VLM-guided zero-shot object goal navigation. But when we analyze the distance to the goal closely, we can see that even though our model is not able to make it a success, the agent is, on average, able to reach the goal more closely and consistently with the proposed models. The comparison of the distance to goal metric for different models is shown in Figure 9. In this section we use object goal navigation annotations on HM3D dataset, from numbers its clear that the object looked as goal by our PixNav model is probably another instance of goal. The detections being validated by DINO its another instance, during the trial the agent tries to reduce distance to this goal. Our agent donot explore the first instance it detects is taken as the goal for PixNav model. This shows indicates that depth module enabled the agent to look for another instance of goal than the annotated one. As the distance to predicted goal or goal passed to proposed PixNav model is $\leq 1m$ they can also be considered a success.

A.8 Performance comparison on edge device

To evaluate the performance of the trained pixel navigation policies on a real robot with power and compute constraints, a performance comparison was conducted on an edge device. The target device used is NVIDIA AGX Orin with the OAK-D Pro sensor. To facilitate real-time testing, a random goal pixel is used to compute the goal mask within each image frame. Now the goal descriptors and the agent's observations at each time step are passed to the trained policy to make a prediction. Maximum steps were limited to 64. For each model, the average time taken to predict an action is tabulated in Table 11. The results show that SSM models with approximately half the model size can predict an action with reduced latency. Given the mean inference time taken for the baseline model, t_b and proposed model t_p, we compute the speed-up percentage as follows,

$$\text{Speed-up} = \frac{t_b - t_p}{t_b} \tag{16}$$

Table 11: **Performance comparison on edge device**. On the selected edge compute and sensor, the models were executed, and the average inference time from a trajectory is reported.

Model	Average step-level inference time (s)	Speed-up
Baseline	0.0847	-
Causal SSM-RGB PixNav	**0.0703**	**0.1700**
Causal SSM-RGBD PixNav with depth gate	0.0770	0.0909

The variation in the time to predict an action at each step in a trajectory is depicted in Figure 10. Through careful modeling that balances reduced model size with improved performance, we find that our proposed models perform with low latency on our compute-constrained target device.

Results show that the mean inference time is reduced by ≈10-15s with the proposed SSM variants. Additionally, these policies achieve a maximum speed-up of 17% for SSM-RGB PixNav, which is very crucial for a mobile agent. In this section, we have evaluated and compared inference time primarily on an edge compute to determine the latency. But in the future, we plan to extend the work to test on real hardware by addressing sim-to-real challenges, including fine-tuning the policy to account for sensor noise, recovery mechanisms, and control.

A.9 Need for causal Mamba variant

Mamba is causal in training sequential data processing. During training, we pass all K observations and jointly calculate the loss. Because the data is not processed sequentially during training, there can be data leakage. During evaluation, execution is sequential. This can adversely affect the model's generalization during evaluation. To address this issue we introduce a mask to ensure the future timestep are masked.

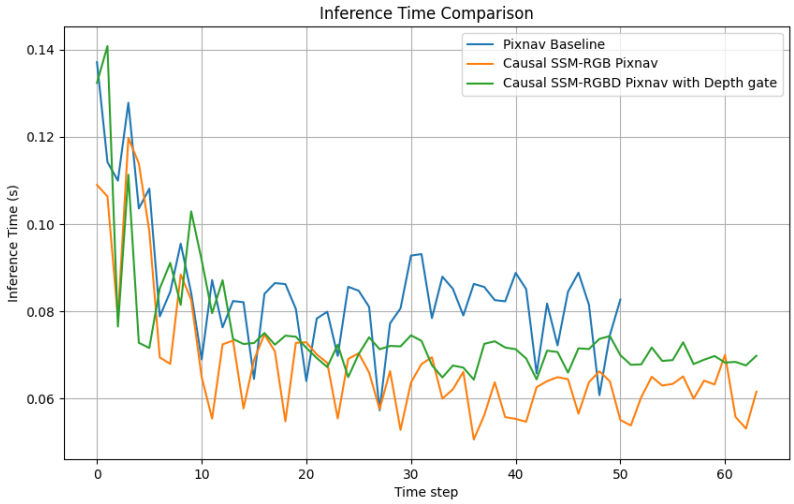

Figure 10: **Inference time comparison**. Time taken to predict an action in all steps taken by an agent in a trajectory with different policies.

A.10 Effect of Depth gate

The depth maps offers geometric awareness to the agent. By introducing depth in Causal SSM-RGBD PixNav the performance is not near to RGB variant. In SSM models as we donot guide when to look at depth data unlike transformers with attention, the depth data confused the model. To this end a depth gate was introduced to learn when to leverage depth. By learning the depth gate parameter, we try to make the model learn, how much to rely on depth. Through this step the depth gated variant bags $\approx 3\%$ improvement in SR. For a trajectory from HM3D during rollout evaluation for each time step, the observations, learned depth gate mixing ratio and predicted goal coordinates are shown in Figure 11. We visualize the learned

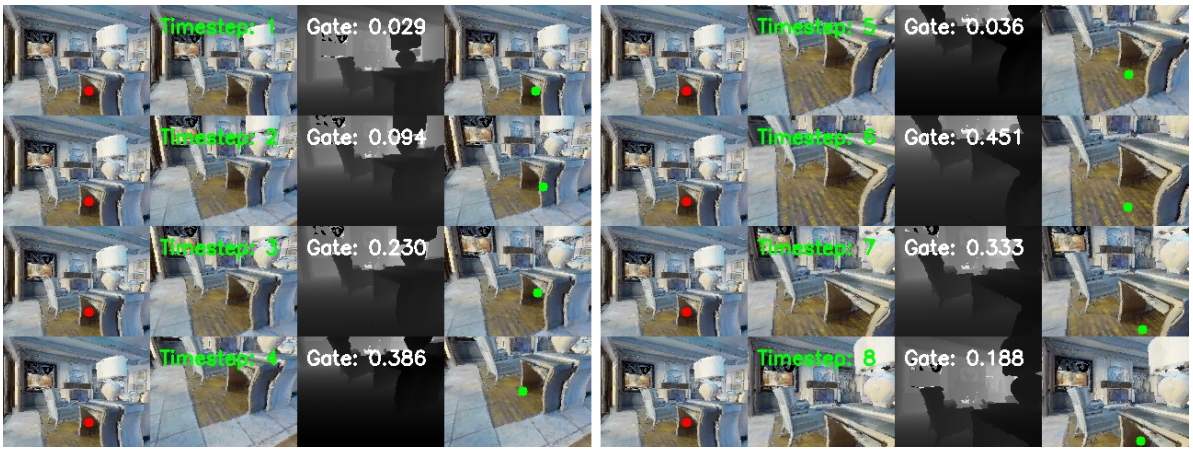

Figure 11: Analyzing the depth gate activations from an episode during rollout evaluation with HM3D with Causal SSM-RGBD PixNav with depth gate. The policy dynamically increases reliance on depth in geometrically complex or cluttered regions, while suppressing it when RGB observations are sufficient. Goal coordinate and predicted goal coordinate for an episode are marked as red and green circles respectively.

depth gating values across timesteps for a representative trajectory. The model assigns low gate values when RGB observations are sufficient (t=1–2), while higher values are observed in cluttered or geometrically

ambiguous regions (t=4–6), indicating increased reliance on depth. This demonstrates that the model adaptively modulates depth usage rather than relying on it uniformly.